CHEMISTRY
A EUROPEAN JOURNAL

DOI: 10.1002/chem.201000995

3rd EuCheMS Chemistry Congress

Detection of Carbocationic Species in Zeolites: Large Crystals Pave the Way

Eli Stavitski,[a] Evgeny A. Pidko,[b] Marianne H. F. Kox,[a] Emiel J. M. Hensen,[b] Rutger A. van Santen,[b] and Bert M. Weckhuysen*[a]

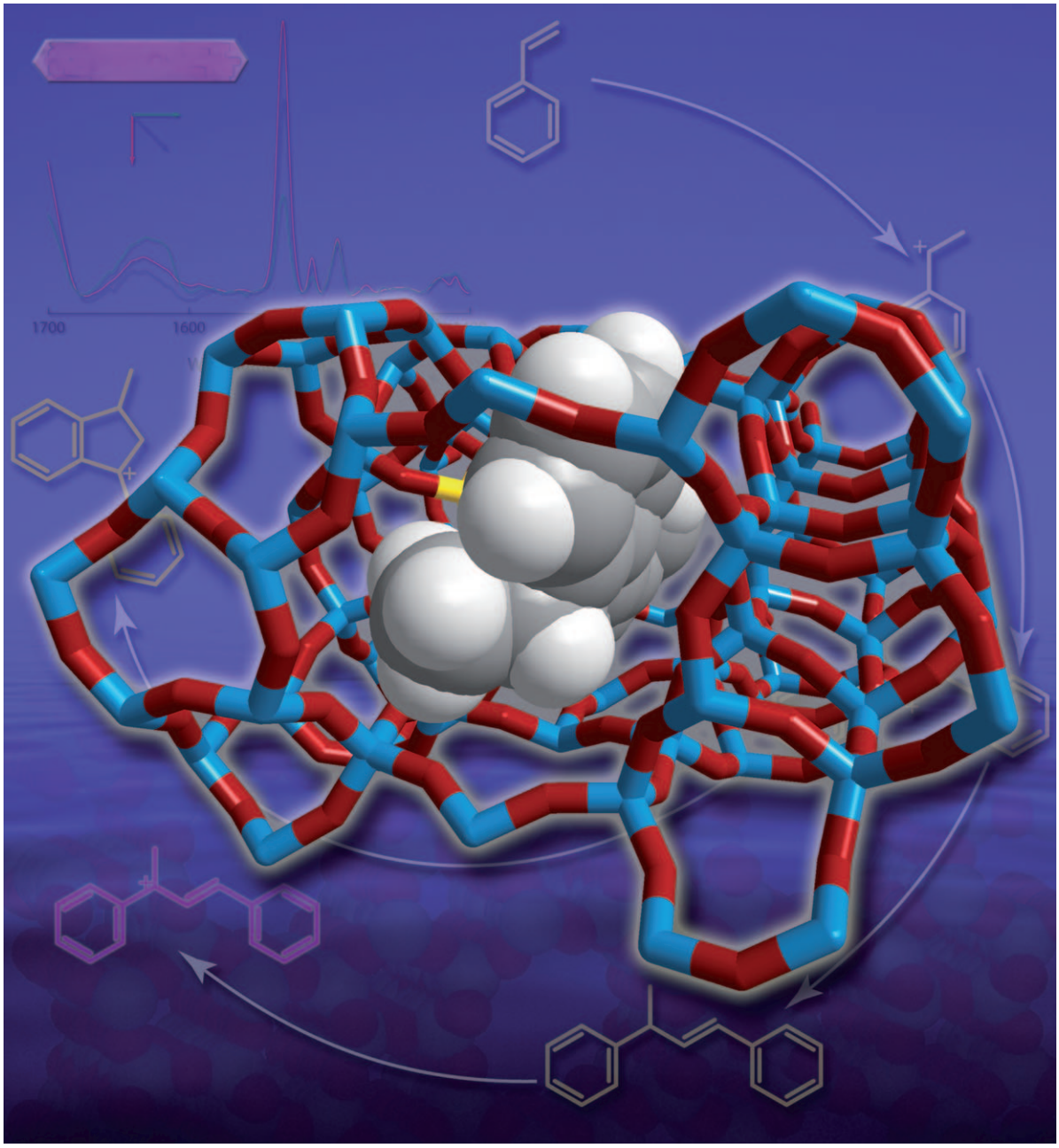

Abstract: Large zeolite crystals have been used as model systems for the investigation of diffusion and catalytic reactivity phenomena in microporous host materials for at least two decades. However, their potential in assisting the detection of elusive reactive intermediates appears to have been underestimated. Herein, we show that a complementary use of vibrational and optical spectroscopy in combination with theoretical calculations allows for the unambiguous identification of transient carbocationic species generated upon the acid-catalyzed oligomerization of styrene derivatives within zeolite H-ZSM-5. Thanks to the mediated diffusion of the reactant in the large H-ZSM-5 crystals and minimal external surface the reaction intermediates can be accumulated within zeolite micropores in sufficient concentrations to allow their detection by synchrotron-based IR microspectroscopy. The UV/Vis and IR spectra display strong polarization dependence of on the molecular alignment of the dimeric styrene carbocations imposed by the zeolite channels and cages that can be rationalized in terms of the electronic and vibrational transitions of the intrazeolite carbocations. Based on these findings, a molecular-level picture of the macroscopic arrangement of the reaction intermediates confined within microporous zeolite matrices can be devised.

Keywords: density functional calculations · microspectroscopy · molecular alignment · oligomerization · zeolites

Introduction

Zeolites and related porous materials are extensively applied as efficient catalysts in various chemical processes.[1–3] A broad spectrum of their application originates from the possibility of fine-tuning their intrinsic chemical and topological properties to match the relevant parameters of a particular catalytic reaction. Rational design of zeolite-based catalyst materials and the fine-tuning of the respective catalytic processes necessitate a deep understanding of the basic aspects of the physicochemical processes underlying the catalytic reactivity of zeolitic materials. Such information can be obtained by a comprehensive investigation of model systems by using various spectroscopic methods. One candidate class of practical models is large zeolite crystals that range in size between tens and hundreds of micrometers. Large crystallites of these dimensions have been synthesized for many zeolite framework types, for example, MFI,[4] FAU,[5,6] BEA,[7] AFI,[8] and LTA.[9,10] Current synthetic methods allow the size, morphology and chemical composition of the resulting particles to be controlled. For example, in a recent report we presented a detailed investigation of the morphology of 18 different types of ZSM-5 and silicalite (both with MFI topology) crystals, varying in their dimensions and internal architecture.[11] Based on this study, a general intergrowth model was proposed, including details on the inner and outer surface boundaries for molecular diffusion.

Long-range order and known pore orientation in large zeolite crystals make it possible to study both diffusion and reactivity in these systems. Naturally, spatially resolved spectroscopic methods with micrometer resolution come in handy for these studies. One of the first successful attempts in which vibrational spectra of *para*-xylene in a large silicalite crystal were recorded with IR microscopy was reported by Schüth.[12] The recorded spectra show strong dependence on the polarization of the incident IR radiation. However, because the intergrowth structure of the MFI crystals had not been accurately determined at the time, the concise interpretation of the results could not have been carried out.[12] Further on, the same method has been applied to investigate the removal of the structure-directing agent template in ZSM-5, and various steps of the process leading to template decomposition were detected.[13] A combination of IR and interference microscopy was employed to follow the diffusion of small organic molecules in zeolites.[14,15] Molecular diffusivity values can be extracted from the analysis of the spatially resolved concentration profiles when combined with molecular modeling.

Large zeolite crystals have also proven to be excellent model systems for reactivity studies. Recently, we presented a multi-technique microspectroscopic approach for studying liquid-phase styrene[16–18] and thiophene[19,20] oligomerization on H-ZSM-5 crystals as probe reactions. By combining UV/Vis, fluorescence, CARS, and IR microscopy, a correlation between local structural features of the zeolite particle and the corresponding catalytic behavior, in terms of styrene/thiophene oligomerization product distribution, was established. In more detail, a nonuniform catalytic activity in two and three dimensions was visualized by using UV/Vis, CARS, and (confocal) fluorescence microscopy,[16,17] and IR microscopy was used to confirm the results and provide insight into the chemical structure of the reaction intermediates.[18] The approach has been further extended to gas-phase reactions, such as the methanol-to-olefin (MTO) conversion.[21]

[a] Dr. E. Stavitski, Dr. M. H. F. Kox, Prof. Dr. B. M. Weckhuysen
Inorganic Chemistry and Catalysis Group
Debye Institute for Nanomaterials Science, Utrecht University
Sorbonnelaan 16, 3584 CA Utrecht (The Netherlands)
Fax: (+31) 30-251-1027
E-mail: b.m.weckhuysen@uu.nl

[b] Dr. E. A. Pidko, Prof. Dr. E. J. M. Hensen, Prof. Dr. R. A. van Santen
Schuit Institute of Catalysis
Laboratory for Inorganic Chemistry and Catalysis
Eindhoven University of Technology
5600 MB Eindhoven (The Netherlands)

Herein, we present a unified view on the acid-catalyzed styrene oligomerization reaction in large ZSM-5 crystals, based on (partly) reported experimental data supported by density functional theory (DFT) calculations. The mechanism of the formation of reaction intermediates in the context of the previously suggested reaction pathways will be discussed. We also aim to demonstrate how the strong polarization dependence of the UV/Vis and IR spectra can be rationalized. In addition, the ability to detect short-lived reaction intermediates is important in establishing the mechanisms of catalytic transformation. In this study, we compare spectroscopic data obtained for large zeolite crystals and powders, which indicate that the unique topological properties of the former allow for the formation of carbocationic transient species in concentrations detectable by UV/Vis and synchrotron-based IR microspectroscopy. This brings an important advantage because it enables the identification of the chemical structure of reactive molecules by correlation of the experimental electronic and vibrational spectra with data from theoretical investigations.

Results and Discussion

We have previously reported on a combination of micro- and spectroscopic methods employed to unravel the mechanism of the styrene transformation within H-ZSM-5 zeolite crystals.[16–18] The primary rationale of this work was to correlate the structure of the different areas of the H-ZSM-5 crystals, in terms of the crystal facet exposed, with the catalytic activity in these regions. The main finding of the UV/Vis microspectroscopic study was the non-uniform distribution of the carbocationic styrene oligomers reaction intermediates throughout different regions of the crystal. Dimeric carbocations were primarily formed at the edges of the crystal, whereas the organic intermediates in the main body of the particles mainly consisted of higher oligomers of styrene. Within the complex intergrowth model, first proposed based on the X-ray diffraction[4] and optical microscopy data and later unambiguously confirmed by the electron backscattering diffraction/focused ion beam (EBSD/FIB) method,[22] these two regions differ in terms of the pore alignment. At the edges, straight pores are open to the surface, whereas in the main body of the crystal they run in parallel to it. This specific alignment of the pore system explains the observation of partial blockage of the straight pores. According to the polarization dependence of the optical absorption, the straight pores contain the oligomers, whereas the zigzag pores interconnecting them play a role in the diffusion of the monomer molecules to the active sites. Furthermore, by probing the same H-ZSM-5/styrene system by synchrotron-based IR microspectroscopy with a spatial resolution close to that of UV/Vis microspectroscopy we were able to detect absorption bands that could only be attributed to the conjugated dimeric carbocation. The species detected are the same species that were assumed to be responsible for the coloration of the H-ZSM-5 crystal during the reaction and the occurrence of an electronic absorption band at $\lambda \approx 540$ nm. This assignment was made based on IR spectra computed by DFT calculations in vacuum of the suspected molecules and suggested that the formation of conjugated linear styrene dimers is associated with a drastic enhancement of the IR band at around $\tilde{\nu} = 1550\ \mathrm{cm}^{-1}$. This band has been experimentally observed in styrene transformations over acidic zeolites. Importantly, a substantial light polarization dependency of this IR band has also been observed. This finding supports the preferred orientation of the conjugated dimerization products within the zeolite channels. Note that the observed polarization dependence does not directly indicate the preferred orientation of the molecular species characterized by the respective IR spectroscopic signatures within the zeolite crystals, but rather the direction of the corresponding dipole transition moments. A proper rationalization of the interplay between the orientation of the reaction intermediates within the zeolite micropores and the experimentally observed light polarization dependencies in IR spectra necessitates an accurate analysis of the respective vibrational modes and the associated transition dipole moments. These factors were not considered in previous work and merit a more detailed investigation, as presented in this work.

The first observation of the optical absorption bands arising when styrene derivatives come into contact with solid acids has been made with microcrystalline catalyst powder.[23] One should expect the appearance of the same IR bands in this case. However, reported experimental spectra (Figure 5 in ref. [24]) do not show an absorption band in the spectral region of $\tilde{\nu} \approx 1550\ \mathrm{cm}^{-1}$, even though the positions of the bands in question had been predicted by DFT.

We ventured to reproduce the experimental results reported by Fernandez et al.[23] with different zeolites, namely, H-ZSM-5 and H-Y, with a broad range of Si/Al ratios. Pellets of zeolite powders were brought into contact with styrene and styrene derivatives at room temperature and subsequently heated to 90 °C. IR spectra were taken at 5 °C increments. At temperatures up to ≈40 °C and depending on the Si/Al ratio, the IR spectra only contained the band of the reagent (Figure 1). At higher temperatures, the charac-

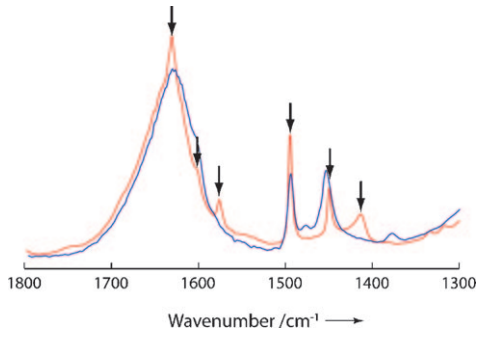

Figure 1. IR spectra of H-ZSM-5 powder (with a Si/Al ratio of 25) exposed to styrene before (red) and after (blue) heating to 60 °C for 2 min. The IR bands, marked with arrows, are assigned to styrene.

teristic styrene bands disappeared and polystyrene IR bands evolve at $\tilde{\nu}=1452$ and 1495 cm^{-1}, indicating the onset of polymerization. However, no IR bands at around $\tilde{\nu}=$ 1550 cm^{-1} were observed, regardless of the zeolite topology or styrene derivative.

The observation that the IR bands of the carbocationic intermediates could not be detected with H-ZSM-5 zeolite powders is in agreement with previous reports[18] and indicates a strong dependence of the reactivity of the catalytic materials on the zeolite morphology. To further substantiate our previously published findings on 4-fluorostyrene, we recorded the IR spectra that arose upon the interaction of styrene and 4-chlorostyrene with large H-ZSM-5 crystals. The IR spectra and their dependence on the light polarization are shown in Figures 2 and 3. One can see that in both cases

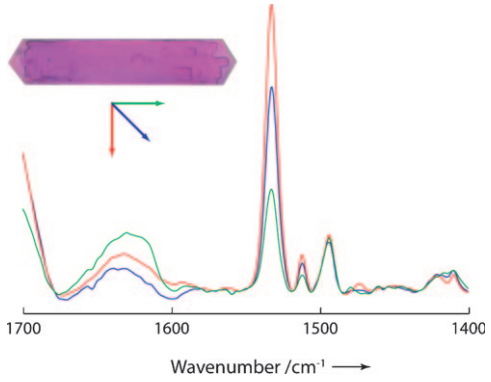

Figure 2. Synchrotron-based IR spectra ($\tilde{\nu}=1400$–1700 cm^{-1} region) of a large H-ZSM-5 crystal in contact with 4-chlorostyrene taken with radiation polarized in different directions as indicated. The spectra are background corrected.[26]

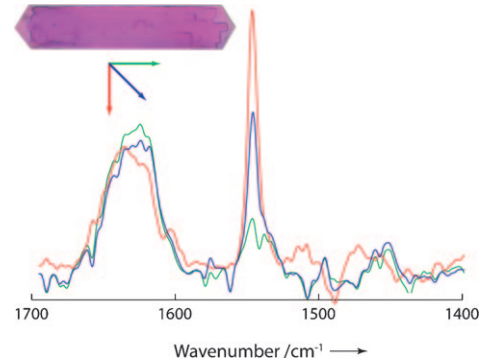

Figure 3. Synchrotron-based IR spectra ($\tilde{\nu}=1400$–1700 cm^{-1} region) of a large H-ZSM-5 crystal in contact with styrene taken with radiation polarized in different directions as indicated. The spectra are background corrected.

a strong IR band appears in the spectral region of $\tilde{\nu}=1540$ to 1550 cm^{-1}, which was previously attributed to the dimeric carbocation.[25] This indicates that large H-ZSM-5 crystals probably exhibit unique properties that allow stabilization of the dimeric carbocations within the nanopores and prevent their further interaction with styrene or other reaction intermediates.

To obtain a better insight into the mechanism of styrene oligomerization and the influence of the zeolite topology on the preferred reaction paths and overall reactivity, we have investigated the thermodynamics of the acid-catalyzed oligomerization of styrene within the micropores of zeolites H-ZSM-5 and H-Y by periodic DFT calculations. Previously, the mechanism of the formation of linear dimeric carbocation **5** and cyclic dimeric carbocation **7** in zeolites was proposed by Corma and García,[24,27] although no detailed justification of the reaction mechanism was provided. Note that because of the steric hindrance of the channel system of zeolite H-ZSM-5, the formation of rigid species **5** in the sinusoidal channel is rather unlikely. Thus, the DFT computations herein were performed only for those reactions within the straight channel of H-ZSM-5. The respective reaction steps and the associated reaction energies for zeolites H-Y and H-ZSM-5 are summarized in Scheme 1. Irrespective of the zeolite topology under consideration, the formation of linear carbocation **3** is strongly exothermic.

A pronounced acidity of the CH_2 group in **3** allows further transformation to give conjugated alkene **4** through the transfer of the acidic H atom to the zeolite lattice. Despite the cleavage of a rather strong C–H bond, this reaction step is exothermic because of the energy gain associated with the electron delocalization in the conjugated π system of **4** and the formation of a rather strong π complex between the resulting alkene and the acidic proton bound to the zeolite framework. Further transformation of **4** to **5** implies a hydride transfer step from the tertiary carbon atom of **4**. This step involves direct interaction between species **4** and **3** confined in the zeolite pores. Note that although a very bulky transition state for such as bimolecular reaction path seems plausible within large faujasite cages, the steric hindrance of the H-ZSM-5 pores will prevent its formation despite the computed exothermicity. An alternative reaction path involves direct formation of **5** through recombination of the hydridic hydrogen atom from the tertiairy carbon of **4** with the zeolitic proton. This dehydration path is quite endothermic. Nevertheless, the entropy gain due to the formation of gaseous H_2 will compensate the endothermicity of the reaction. Indeed, estimations of the Gibbs free energy changes at 373 K for the convential bimolecular (**4**+**3**→**5**+**6**, −33 kJ mol^{-1}) and the direct (**4**→**5**+H_2, −45 kJ mol^{-1}) paths within the narrow pores of ZSM-5 suggest that under these reaction conditions the direct hydride transfer mechanism is favored. Importantly, this result changes when the reaction takes place within the larger faujasite supercages. In this case, the Gibbs free energy of the bimolecular hydride transfer (−68 kJ mol^{-1}) compares very favorably with the values computed for the direct path (−45 kJ mol^{-1}). This suggests a strong influence of the zeolite topology and the associated steric properties in the vicinity of the reaction site on the preferred mechanism of the reaction.

Besides the formation of conjugated linear carbocation **5**, there is a competing path for the transformation of **3** that

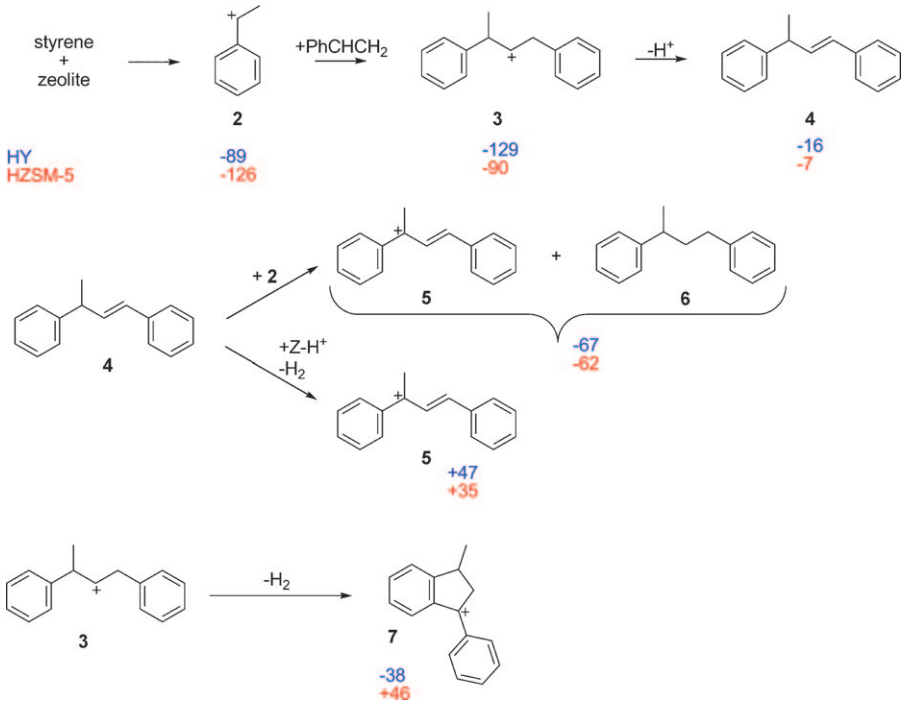

Scheme 1. The reaction pathways of styrene on acidic zeolite materials and the respective DFT-computed reaction energies in kJ mol^{-1}.[28]

leads to the formation of cyclic carbocationic product **7** followed by further styrene oligomerization. This reaction implies a substantial increase in the bulkiness of the hydrocarbon species. As a result, the reaction path leading to the formation of cyclic species **7** is strongly preferred within the larger voids of zeolite H-Y. These carbocations do not form inside the smaller pores of H-ZSM-5. Indeed, the UV/Vis studies indicate the exclusive formation of cyclic species **7** upon styrene oligomerization in Y zeolite.[28] When the reaction takes place in large H-ZSM-5 crystals, linear carbocations are the predominant products, whereas cyclic products are also observed as the zeolite crystal size decreases. One expects that smaller zeolite crystals contain a larger fraction of acid sites within "defect" and imperfect environments in the vicinities of the crystal borders. As a result, the steric constraints at such sites are substantially reduced and thus allow the formation of cyclic product **7**.

The DFT results presented above indicate the possibility of **5** forming within the straight pores of zeolite H-ZSM-5. The question remains whether the orientation of these linear conjugated carbocations explains the experimentally observed light polarization dependency of the UV/Vis and synchrotron-based IR spectra. Time-dependent DFT calculations on species **5** indicate the presence of two lowest energy electron transitions at $\lambda = 537$ and 513 nm, which correspond to HOMO−1→LUMO and HOMO−2→LUMO transitions, respectively. This is illustrated in Figure 4. The computed values of the excitation energies are in line with the experimental UV/Vis spectroscopic results. The shape of the respective molecular orbitals (Figure 4) suggests that the direction of the polarization dependency observed in the UV/Vis spectra correlates to the direction of the long molecular axis of hydrocarbon intermediate **5** within the zeolite crystals. We must, however, note that the TD-DFT results on these systems show very strong method and model dependency and, therefore, can only be used as a qualitative tool for deducing the preferred orientation of carbocationic species within zeolite micropores.

A more in-depth theoretical analysis can be performed by analyzing the vibrational properties of linear conjugated carbocations **5** in the gas phase and confined in the ZSM-5 channels. Indeed, the formation of a positive charge within a delocalized π system of **5** is expected to have a profound effect on the IR spectra. The C–C vibrations involving carbon atoms of the allylic fragment that have a positive charge should show a very strong transition dipole moment. Furthermore, the rigidity of the molecular unit results in a very strong directionality of the associ-

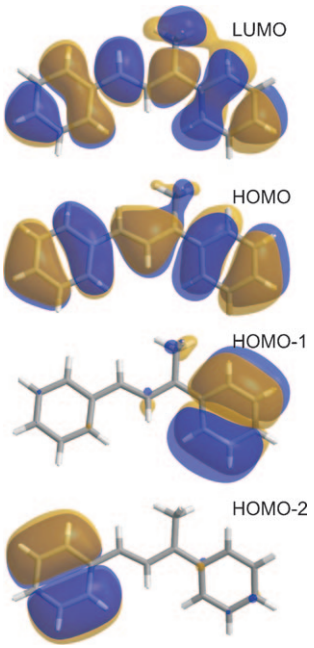

Figure 4. Frontier molecular orbitals (PBE/6-311G(d,p), isovalue 0.01) for conjugated carbocation **5** formed during the acid-catalyzed oligomerization of styrene within zeolites.

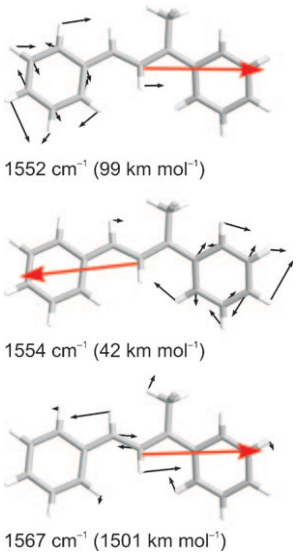

Figure 5. DFT (PBE/6-311G(d,p)-computed vibrational modes for conjugated carbocation **5** in the gas phase, with the corresponding atomic displacements and dipole derivative unit vector (transition dipole moment) shown as black and red arrows, respectively.

ated dipole-derivative vector. Thus, when such species are confined within ordered microporous channels of ZSM-5, the respective IR spectra should show a very strong polarization dependency.

DFT calculations predict a dramatic intensity enhancement of the IR band at $\tilde{\nu}=1567\ \mathrm{cm}^{-1}$ that is mainly contributed by the displacements of the allylic C atoms of **5** (Figure 5). The dipole derivative vector of this vibration is parallel to the long molecular axes of the carbonation. Furthermore, other DFT-computed vibrations with frequencies that fall in the range of the experimentally observed bands attributed to the formation of **5** in H-ZSM-5 also show the same directionality of the transition dipole moment. Thus, the polarization dependence of the IR spectra can be correlated with the orientation of molecular species **5** within the zeolite crystals.

Analysis of the dynamic dipole moment associated with molecular vibrations of **5** within H-ZSM-5 micropores indicates that the direction of the transition dipole moment is not influenced by confinement in the zeolite matrix (Figure 6). Note that the shape of the vibration modes computed for unsubstituted carbocation **5** in H-ZSM-5 zeolite differs slightly from those calculated for the gas-phase species. For the adsorbed species, the contribution of the C–C stretch at the carbocationic center is more pronounced for all three vibrations, although the general picture is the same. The stronger contribution of the C–C stretch of the allylic moiety results in a more substantial intensity enhancement of the associated vibrational modes (Figure 6). Vibrational properties of the linear conjugated dimeric carbocations that are formed upon dimerization of Cl- or F-substituted styrene do not show qualitative deviations from the findings for unsubstituted species **5**. The presence of Cl and F sub-

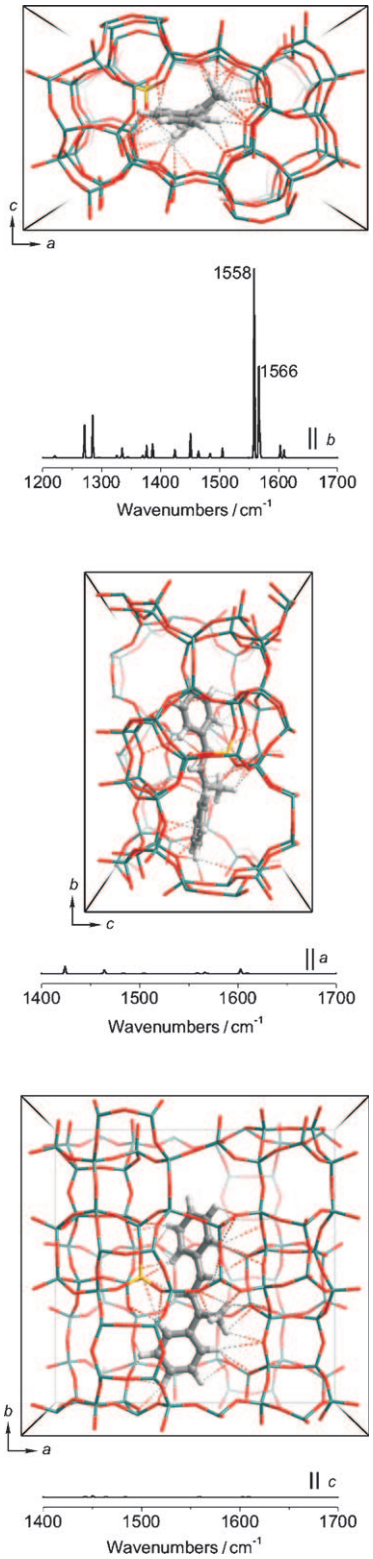

Figure 6. Optimized geometry of linear conjugated carbocation **5** formed during styrene oligomerization in the straight channel of H-ZSM-5 (projections parallel to crystallographic axes are shown). DFT-computed infrared spectra with the intensities estimated from the dynamic dipole moment were only considered in parallel to the corresponding crystallographic axes.

stituents at the *para*-positions of the phenyl moieties of **5** leads to red- and blueshifts of the relevant vibrations (Table 1). This agrees well with the experimental observations.

Table 1. DFT-computed and experimental vibrational frequencies for substituted and unsubstituted delocalized linear styrene carbocations formed within HZSM-5 zeolite channels.

	Unsubstituted	F-substituted	Cl-substituted
Calculated	1568	1578	1553
	1566	1570	1548
	1558	1560	1538
Experimental	1542	1534	1531

In light of the above discussion, it is interesting to compare the previously reported optical spectra of the ZSM-5 large crystals[17] and powders[28] recorded after 4-fluorostyrene oligomerization. Note that in the latter case, an absorption band at $\lambda = 490$ nm can be identified from the deconvolution of the spectra irrespective of the Si/Al ratio, whereas optical absorption in this spectral region is negligible for large crystals. These UV/Vis bands were proposed to originate from cyclic carbocation **7** and were observed in zeolite Y.[28] In a FAU structure, supercages favor the formation of the cyclic carbocations. In the MFI framework, the cyclic structures can only form in the open sites near the crystallites surface and mesopores where special constrains in the channels are alleviated. Thus, the long-range order attainable with large crystals is essential to be able to differentiate between different reaction intermediates.

Conclusion and Outlook

Herein we have used UV/Vis and synchrotron-based IR microspectroscopy and complementary theoretical analysis to demonstrate how the unique properties of large zeolite crystals allow the detection of reactive intermediates, which are difficult, if not impossible, to pinpoint in regular zeolite powders. Mediated activity and diffusion within the micron-sized zeolite crystals along with the minimized external surface area are the key factors that allow the reaction to be quenched and the highly reactive species to be investigated by spectroscopic means. The complementary use of microspectroscopy and computational modeling has been shown to be essential for the identification of intermediates in the Brønsed-acid-catalyzed oligomerization of styrene derivatives. Moreover, the macroscopic alignment of the styrene-derived molecules in the zeolite channels and a deep insight into the microscopic topology of the zeolite crystals can be determined by using this approach.

We believe that there are a multitude of classical catalytic processes that can be mechanistically investigated in great detail with large zeolite crystals as model catalysts, and a wide variety of powerful microspectroscopic methods are nowadays available to accomplish these tasks.[29] It should be pointed out that the necessity of a combination of microspectroscopy and theory has been highlighted before by Schoonheydt, that is, a successful implementation of a method that fuses experimental and theoretical research can potentially contribute to the research in the field of zeolites in particular and heterogeneous catalysis in general.[29b]

Experimental Section

Materials: H-ZSM-5 and H-Y zeolite powders (Zeolyst CBV series, with Si/Al ratios of 11–40 and 2.5–40, respectively) were calcined at 600 °C for 2 h before measurements. For IR measurements, the zeolite powders were pressed into self-supporting wafers (15 mg cm^{-2}). Large ZSM-5 crystals (with a Si/Al ratio of 17) were provided by Exxon–Mobil (Machelen, Belgium). The zeolite in its sodium form was triple ion-exchanged with aqueous ammonium nitrate, dried, and calcined. Styrene, 4-chlorostyrene, and 4-fluorostyrene (Acros Organics) were used as received. Zeolite crystals were exposed to styrene and its derivatives and heated in an in situ cell (FTIR 600, Linkam Scientific Instruments) equipped with a temperature controller (TMS 93). Prior to the measurements, the crystals were pretreated at 200 °C for 30 min inside the cell. Note that this temperature is not sufficiently high to remove all adsorbed water, which can result in the appearance of an IR band at $\tilde{\nu} = 1630$ cm^{-1}; however, in our previous experiments we did not observe any difference in the spectral intensity regardless of whether the activation was carried out at 200 °C or at temperatures up to 500 °C.

IR spectroscopy: Infrared spectra of the zeolite powders exposed to styrenes were recorded by using a Perkin–Elmer FTIR spectrometer. FTIR microspectroscopic experiments were performed at beam line U10B at the National Synchrotron Light Source (NSLS), Brookhaven National Laboratory (Upton, NY, USA). A Thermo Nicolet Magna 860 FTIR spectrometer coupled to a Continuum IR microscope (Thermo Nicolet, Madison, WI, USA) was used with synchrotron light as the infrared source. The microscope was equipped with a ×32 Schwarzschild objective, a motorized *x*–*y* mapping stage, an adjustable rectangular aperture, and a liquid-nitrogen-cooled mercury–cadmium–telluride detector. A transflectance spectrum was recorded in reflectance mode in the mid-infrared spectral range ($\tilde{\nu} = 4000$–800 cm^{-1}) with a spectral resolution of 4 cm^{-1} and 64 scans co-added. The IR beam (aperture) size used was 5 × 5 μm. Spectra were taken from the center of the crystal.

DFT calculations: Thermodynamics of styrene oligomerization in zeolite micropores was studied by using the Vienna Ab Initio Simulation Package (VASP) within density functional theory (DFT).[30] The gradient-corrected PBE exchange-correlation functional was used.[31] Electron–ion interactions were described with the projected-augmented wave (PAW) method[32,33] and for valence electrons a plane wave basis set was applied. The energy cut-off was set to 400 eV. The Brillouin zone sampling was restricted to Γ-point.[34] In the first step, the cell parameters were optimized for the periodic models of full-silica zeolite crystals. DFT-computed reaction energies were corrected for van der Waals interactions by computing an additional interatomic Lennard–Jones potential for the DFT-optimized structures as defined in the CVFF (consistent valence force field)[35,36] with the approach proposed by Demuth et al.[37] and Vos et al.[38] by using the GULP program.[39] Gibbs free energies were computed within the ideal gas approximation at a pressure of 1 atm and a temperature of 373 K by using the results of frequency analysis performed by means of the finite difference method as implemented in VASP. Periodically repeated crystallographic unit cells of zeolites MFI and Faujasite were used as models. In the former case the orthorhombic structure of ZSM-5 was used.[40] The parameters of the all-silica MFI orthorhombic structure ($Si_{96}O_{192}$) after optimization of volume and shape were as follows: $a = 20.119$, $b = 19.767$, $c = 13.161$ Å. By replacing one of the 96 unit cell silicon atoms by an aluminum atom, an MFI lattice with a

Si/Al ratio of 95 was obtained. The aluminum atom was positioned at the T2 crystallographic site, which creates an acid site at the intersection of the straight channel and the sinusoidal pore. To test the effect of the relative location of the confined carbocationic species and the framework Al distribution on the polarization dependency of vibrational spectra, we also calculated an MFI model that was created by introducing an Al substitution at the MFI T7 site at the channel intersection distant to that used in the original model, while the confined carbocationic species remained at the same position as in the original optimized model of **5**. Geometry optimization of the resulting structure led to a substantially different orientation of the confined carbocation relative to the anionic framework T7 site, as compared to the situation for the T2/Al substitution. Nevertheless, the general picture observed in the computed vibrational spectra and their polarization dependency were not notably affected by the different framework. A hydrogen atom, which introduced a Brønsted-acid site, was implemented into the structure to obtain a neutral framework. Similarly to out previous studies,[41,42] the periodic model of zeolite H-Y was a rhombohedral faujasite unit cell ($Si_{48}O_{96}$). The following optimized parameters of the all-silica zeolite Y rhombohedral unit cell were calculated: $a=b=c=17.5125$ Å, $\alpha=\beta=\gamma=60.00°$. 14 silicon atoms were replaced by aluminum atoms that were uniformly distributed over the unit cell according to the Löwenstein rule. This resulted in a Si/Al ratio of 2.43. To compensate the resulting negative charge on the framework, 14 hydrogen atoms were introduced to the structure. Further details of the computational procedures and zeolite models used can be found elsewhere.[28] Gas-phase geometry optimization, vibrational analysis, and TD-DFT calculations on the conjugated carbocationic styrene dimers were performed at the PBE/6–311G(d,p) level by using the Gaussian 03 program package.[43]

Acknowledgements

We thank the Dutch National Science Foundation (NWO-CW VICI, VENI and TOP grant) and Research School Combination Catalysis (NRSC-C) for financial support. Dr. Machteld Mertens (ExxonMobil, Machelen, Belgium) is acknowledged for providing the large ZSM-5 crystals.

[1] J. Weitkamp, L. Puppe, *Catalysis and Zeolites: Fundamentals and Applications*, Springer, Heidelberg, **1999**.
[2] A. Corma, *Chem. Rev.* **1997**, *97*, 2373.
[3] *Zeolites and Catalysis: Synthesis Reactions and Applications* (Eds.: J. Cejka, A. Corma, S. Zones), Wiley-VCH, Weinheim, **2010**.
[4] G. D. Price, J. J. Pluth, J. V. Smith, J. M. Bennett, R. L. Patton, *J. Am. Chem. Soc.* **1982**, *104*, 5971.
[5] S. Ferchiche, J. Warzywoda, A. Sacco, *Int. J. Inorg. Mater.* **2001**, *3*, 773.
[6] J. Warzywoda, N. Bac, A. Sacco, *J. Cryst. Growth* **1999**, *204*, 539.
[7] J. Sun, G. S. Zhu, Y. L. Chen, J. X. Li, L. F. Wang, Y. Peng, H. Li, S. L. Qiu, *Microporous Mesoporous Mater.* **2007**, *102*, 242.
[8] E. Lehmann, C. Chmelik, H. Scheidt, S. Vasenkov, B. Staudte, J. Karger, F. Kremer, G. Zadrozna, J. Kornatowski, *J. Am. Chem. Soc.* **2002**, *124*, 8690.
[9] A. S. Huang, J. Caro, *Microporous Mesoporous Mater.* **2010**, *129*, 90.
[10] S. Qiu, J. Yu, G. Zhu, O. Terasaki, Y. Nozue, W. Pang, R. Xu, *Microporous Mesoporous Mater.* **1998**, *21*, 245.
[11] L. Karwacki, M. H. F. Kox, D. A. M. de Winter, M. R. Drury, J. D. Meeldijk, E. Stavitski, W. Schmidt, M. Mertens, P. Cubillas, N. John, A. Chan, N. Kahn, S. R. Bare, M. Anderson, J. Kornatowski, B. M. Weckhuysen, *Nat. Mater.* **2009**, *8*, 959.
[12] F. Schüth, *J. Phys. Chem.* **1992**, *96*, 7493.
[13] M. Nowotny, J. A. Lercher, H. Kessler, *Zeolites* **1991**, *11*, 454.
[14] L. Heinke, C. Chmelik, P. Kortunov, D. M. Ruthven, D. B. Shah, S. Vasenkov, J. Karger, *Chem. Eng. Technol.* **2007**, *30*, 995.
[15] P. V. Kortunov, L. Heinke, M. Arnold, Y. Nedellec, D. J. Jones, J. Caro, J. Karger, *J. Am. Chem. Soc.* **2007**, *129*, 8041.
[16] M. H. F. Kox, E. Stavitski, B. M. Weckhuysen, *Angew. Chem.* **2007**, *119*, 3726; *Angew. Chem. Int. Ed.* **2007**, *46*, 3652.
[17] E. Stavitski, M. H. F. Kox, B. M. Weckhuysen, *Chem. Eur. J.* **2007**, *13*, 7057.
[18] E. Stavitski, M. H. F. Kox, I. Swart, F. M. F. de Groot, B. M. Weckhuysen, *Angew. Chem.* **2008**, *120*, 3599; *Angew. Chem. Int. Ed.* **2008**, *47*, 3543.
[19] M. H. F. Kox, K. F. Domke, J. P. R. Day, G. Rago, E. Stavitski, M. Bonn, B. M. Weckhuysen, *Angew. Chem.* **2009**, *121*, 9152; *Angew. Chem. Int. Ed.* **2009**, *48*, 8990.
[20] M. H. F. Kox, A. Mijovilovich, J. J. H. B. Sättler, E. Stavitski, B. M. Weckhuysen, *ChemCatChem* **2010**, *2*, 473.
[21] D. Mores, E. Stavitski, M. H. F. Kox, J. Kornatowski, U. Olsbye, B. M. Weckhuysen, *Chem. Eur. J.* **2008**, *14*, 11320.
[22] E. Stavitski, M. R. Drury, D. A. M. de Winter, M. H. F. Kox, B. M. Weckhuysen, *Angew. Chem.* **2008**, *120*, 5719; *Angew. Chem. Int. Ed.* **2008**, *47*, 5637.
[23] V. Fornes, H. Garcia, V. Marti, L. Fernandez, *Tetrahedron* **1998**, *54*, 3827.
[24] L. Fernández, V. Marti, H. Garcia, *Phys. Chem. Chem. Phys.* **1999**, *1*, 3689.
[25] Please note that the highest intensity of the band at $\tilde{\nu}=1540$–$1550\ cm^{-1}$ is observed when the IR light polarization is perpendicular to the long axis of the crystal (similar to the dependence of the UV/Vis spectrum as shown, for example, in refs. [16] and [17]), which is in contrast to our previous report.[18] The polarization of the infrared synchrotron beam was incorrectly determined in the previous work.
[26] Note that even in the case when the light polarization is perpendicular to the straight pore orientation, the intensity of the band at $\tilde{\nu}=1530\ cm^{-1}$ does not reach zero. This is due to a combination of two factors. First, it is reasonable to assume that the orientation of the molecules is not exactly parallel to the straight pores, assuming some tilting angle. Second, the entire volume of the crystal is probed in the transflectance mode. In some subunits of the crystals the orientation of the crystallographic axes differs from that in the upper subunit (for a description of the crystal architecture, see ref. [11]). However, relative contributions of these factors are hard to accurately quantify.
[27] A. Corma, H. Garcia, *Top. Catal.* **1998**, *6*, 127.
[28] I. L. C. Buurmans, E. A. Pidko, J. M. de Groot, E. Stavitski, R. A. van Santen, B. M. Weckhuysen, *Phys. Chem. Chem. Phys.* **2010**, *12*, 7032–7040.
[29] a) B. M. Weckhuysen, *Angew. Chem.* **2009**, *121*, 5008; *Angew. Chem. Int. Ed.* **2009**, *48*, 4910; b) R. A. Schoonheydt, *Angew. Chem.* **2008**, *120*, 9328; *Angew. Chem. Int. Ed.* **2008**, *47*, 9188.
[30] G. Kresse, J. Furthmuller, *Phys. Rev. B* **1996**, *54*, 11169.
[31] J. P. Perdew, K. Burke, M. Ernzerhof, *Phys. Rev. Lett.* **1996**, *77*, 3865.
[32] P. E. Blöchl, *Phys. Rev. B* **1994**, *50*, 17953.
[33] G. Kresse, D. Joubert, *Phys. Rev. B* **1999**, *59*, 1758.
[34] H. J. Monkhorst, J. D. Pack, *Phys. Rev. B* **1976**, *13*, 5188.
[35] P. Dauber-Osguthorpe, V. A. Roberts, D. J. Osguthorpe, J. Wolff, M. Genest, A. T. Hagler, *Proteins Struct. Funct. Genet.* **1988**, *4*, 31.
[36] D. H. Kitson, A. T. Hagler, *Biochemistry* **1988**, *27*, 7176.
[37] T. Demuth, L. Benco, J. Hafner, H. Toulhoat, F. Hutschka, *J. Chem. Phys.* **2001**, *114*, 3703.
[38] A. M. Vos, X. Rozanska, R. A. Schoonheydt, R. A. van Santen, F. Hutschka, J. Hafner, *J. Am. Chem. Soc.* **2001**, *123*, 2799.
[39] J. D. Gale, *Z. Kristallogr.* **2005**, *220*, 552.
[40] H. van Koningsveld, *Acta Crystallogr. Sect. B* **1990**, *46*, 731.
[41] P. Mignon, E. A. Pidko, R. A. Van Santen, P. Geerlings, R. A. Schoonheydt, *Chem. Eur. J.* **2008**, *14*, 5168.
[42] E. A. Pidko, P. Mignon, P. Geerlings, R. A. Schoonheydt, R. A. van Santen, *J. Phys. Chem. C* **2008**, *112*, 5510.
[43] Gaussian 03, Revision D.01, M. J. Frisch, G. W. Trucks, H. B. Schlegel, G. E. Scuseria, M. A. Robb, J. R. Cheeseman, J. A. Montgomery, Jr., T. Vreven, K. N. Kudin, J. C. Burant, J. M. Millam, S. S. Iyengar, J. Tomasi, V. Barone, B. Mennucci, M. Cossi, G. Scalmani, N. Rega, G. A. Petersson, H. Nakatsuji, M. Hada, M. Ehara, K.

Toyota, R. Fukuda, J. Hasegawa, M. Ishida, T. Nakajima, Y. Honda, O. Kitao, H. Nakai, M. Klene, X. Li, J. E. Knox, H. P. Hratchian, J. B. Cross, V. Bakken, C. Adamo, J. Jaramillo, R. Gomperts, R. E. Stratmann, O. Yazyev, A. J. Austin, R. Cammi, C. Pomelli, J. W. Ochterski, P. Y. Ayala, K. Morokuma, G. A. Voth, P. Salvador, J. J. Dannenberg, V. G. Zakrzewski, S. Dapprich, A. D. Daniels, M. C. Strain, O. Farkas, D. K. Malick, A. D. Rabuck, K. Raghavachari, J. B. Foresman, J. V. Ortiz, Q. Cui, A. G. Baboul, S. Clifford, J. Cioslowski, B. B. Stefanov, G. Liu, A. Liashenko, P. Piskorz, I. Komaromi, R. L. Martin, D. J. Fox, T. Keith, M. A. Al-Laham, C. Y. Peng, A. Nanayakkara, M. Challacombe, P. M. W. Gill, B. Johnson, W. Chen, M. W. Wong, C. Gonzalez, J. A. Pople, Gaussian, Inc., Wallingford CT, **2004**.

Received: April 17, 2010
Published online: July 6, 2010

